Research Article

Nataliia S. Vorobeva, Saman Bagheri, Angel Torres and Alexander Sinitskii*

Negative photoresponse in $Ti_3C_2T_x$ MXene monolayers

https://doi.org/10.1515/nanoph-2022-0182
Received March 27, 2022; accepted June 20, 2022;
published online July 14, 2022

Abstract: Two-dimensional transition metal carbides, nitrides, and carbonitrides, collectively known as MXenes, are finding numerous applications in many different areas, including optoelectronics and photonics, but there is limited information about their intrinsic photoresponse. In this study, we investigated the visible and near-infrared range photoresponse of $Ti_3C_2T_x$, the most popular MXene material to date. The electrical measurements were performed on devices based on individual monolayer $Ti_3C_2T_x$ MXene flakes, which were characterized by a variety of microscopic and spectroscopic methods. For MXene devices with different electrode layouts, the current reproducibly decreased under illumination with either white light or lasers with different wavelengths in the visible and near-infrared region, thus demonstrating a negative photoresponse. The understanding of the intrinsic photoresponse of $Ti_3C_2T_x$ should facilitate the optoelectronic and photonic applications of MXenes.

Keywords: MXenes; negative photoresponse; $Ti_3C_2T_x$; titanium carbide.

1 Introduction

MXenes are a rapidly growing family of two-dimensional (2D) transition metal carbides, nitrides, and carbonitrides that are finding numerous applications in many different areas ranging from energy storage and electromagnetic interference shielding to gas sensing and biomedicine [1]. There is also an active discussion of the potential use of MXenes for optoelectronic applications, such as photodetectors, phototransistors, and solar cells [2–7]. In many of the reported optoelectronic devices, MXenes were used in combination with various semiconductor materials, such as TiO_2 [8], CdS [9], MoS_2 [10], $CH_3NH_3PbI_3$ perovskite [11], ZnO [12], and others. Several of these devices demonstrated enhanced characteristics or intriguing physical properties, such as a negative photoresponse in photodetectors based on combinations of $Ti_3C_2T_x$ MXene with CdS [9] and MoS_2 [10]. However, when analyzing the behavior of heterostructural or composite materials it is imperative to fully understand the intrinsic properties of their individual components, and while the optoelectronic properties of the above semiconductors have been extensively studied, there is limited information on the intrinsic photoresponse of MXenes.

In this study, we investigated the visible and near-infrared range photoresponse of $Ti_3C_2T_x$ (T_x corresponds to the surface termination of the 2D Ti_3C_2 sheets), the most popular MXene material to date [13]. We performed the measurements on individual $Ti_3C_2T_x$ flakes to exclude the interfacial phenomena at the contacts between the MXene flakes in their bulk assemblies, such as thin films. The measurements showed that devices based on individual monolayer $Ti_3C_2T_x$ MXene flakes exhibit a negative photoresponse, *i.e.* the current decreased when the devices were illuminated with either white light or a laser in the visible or near-infrared range of spectrum. This effect is very different from the behavior previously observed for the partially oxidized $Ti_3C_2T_x$ MXene, in which the presence of TiO_2, a wide bandgap semiconductor, resulted in a positive photoresponse to ultraviolet (UV) light, so that the device current increased under illumination [8]. Consequently, the understanding of the intrinsic photoresponse of $Ti_3C_2T_x$ will be beneficial for designing new MXene composites with other semiconductor materials for a variety of optoelectronic applications [2–4].

***Corresponding author: Alexander Sinitskii**, Department of Chemistry and Nebraska Center for Materials and Nanoscience, University of Nebraska – Lincoln, Lincoln 68588, NE, USA,
E-mail: sinitskii@unl.edu. https://orcid.org/0000-0002-8688-3451
Nataliia S. Vorobeva, Saman Bagheri and Angel Torres, Department of Chemistry and Nebraska Center for Materials and Nanoscience, University of Nebraska – Lincoln, Lincoln 68588, NE, USA

2 Experimental section

2.1 Synthesis of $Ti_3C_2T_x$ MXene

Ti (99%, 325 mesh), Al (99%, 325 mesh), and TiC (99.9%, 325 mesh) were purchased from Alfa Aesar. HCl was purchased from VWR, and LiF was purchased from Spectrum Chemical. All chemicals were used as received. Ti_3AlC_2 MAX phase was synthesized using the 2:1:1.2 M ratio of TiC:Ti:Al. All precursors were mixed using a pestle and mortar, pressed into a pellet at 3500 psi, and annealed at 1450 °C for 8 h under the flow of argon (300 sccm). After the synthesis, Ti_3AlC_2 MAX phase was crushed and sieved to collect uniformly sized particles.

$Ti_3C_2T_x$ MXene was synthesized by the minimally intensive layer delamination (MILD) method [14]. In brief, the MAX phase (500 mg, particle size below 38 μm) was slowly dispersed in the mixture of LiF (800 mg) and 10 mL of HCl (9 M), and stirred for 24 h (600 rpm, 25 °C). The sample was washed and centrifuged until pH 6 was reached and then delaminated into flakes by shaking for 15 min. Finally, the shaken solution was centrifuged (3500 rpm, 30 min), and single-layer flakes in the supernatant were stored at 4 °C for further experiments.

2.2 Materials characterization

Scanning electron microscopy (SEM) was performed using a FEI Nova NanoSEM instrument at the accelerating voltage of 5 kV. Raman spectra of $Ti_3C_2T_x$ MXene were recorded using a Thermo Scientific DXR Raman microscope with a 532 nm excitation laser. Transmission electron microscopy (TEM) and selected area electron diffraction (SAED) of $Ti_3C_2T_x$ flakes were performed using a FEI Tecnai Osiris scanning transmission electron microscope equipped with a HAADF detector and an X-FEG high brightness Schottky field-emission gun; the accelerating voltage was 200 kV. Powder X-ray diffraction (XRD) patterns were collected using a Rigaku Smart Lab powder diffractometer with Ni-filtered Cu Kα radiation operated at 40 kV and 30 mA, using 0.03° step and 3 s dwelling time. Ultraviolet–visible–near infrared (UV–vis–NIR) absorption spectrum of an aqueous solution of $Ti_3C_2T_x$ MXene flakes was recorded using a Jasco V-670 spectrophotometer. Atomic force microscopy (AFM) of $Ti_3C_2T_x$ MXene devices was performed with a Bruker Dimension Icon atomic force microscope using PeakForce Tapping mode.

2.3 Device fabrication and electrical measurements

A droplet of an aqueous solution of $Ti_3C_2T_x$ MXene flakes was placed on a surface of a p-doped Si substrate covered with a 300-nm-thick layer of SiO_2. The droplet was dried in air, resulting in $Ti_3C_2T_x$ MXene flakes dispersed over the Si/SiO_2 substrate. A Zeiss Supra 40 field-emission scanning electron microscope and a Raith pattern generator were used for electron beam lithography (EBL) to pattern electrodes on the $Ti_3C_2T_x$ MXene flakes. An AJA electron beam evaporator at the base pressure of $\sim 8 \times 10^{-9}$ Torr was used to evaporate 3 nm of Cr and then 20 nm of Au, both at the 0.02 nm/s rate.

The $Ti_3C_2T_x$ MXene devices were measured in a Lake Shore TTPX cryogenic probe station at the base pressure of about 2×10^{-6} Torr. Prior to the electrical measurements, the devices were kept in the evacuated chamber of a probe station for at least 2 days to minimize the effect of surface adsorbates [15]. The electrical measurements were performed using an Agilent 4155C semiconductor parameter analyzer that was operated using a National Instruments LabView code.

For the white light illumination of the $Ti_3C_2T_x$ MXene devices, we used a 150 W Philips 14,501 DDL 20 V halogen light bulb; the emission spectrum of this bulb was reported elsewhere [16]. A Thorlabs S120C standard photodiode power sensor was used to measure the maximum light intensity at 600 nm of 6 mW cm^{-2}.

For the wavelength-dependent photoconductivity measurements, we used a Thorlabs multichannel laser source with 517 nm (green), 686 nm (red), and 965 nm (infrared) outputs. For each laser, the power was standardized at 3.5 mW. A laser spot with a diameter of about 5 mm was aligned on a $Ti_3C_2T_x$ MXene device using an optical fiber.

3 Results and discussion

The inset in Figure 1a shows the structure of a monolayer $Ti_3C_2T_x$ MXene flake. The flake contains three hexagonal layers of titanium atoms arranged in the cubic close-packed arrangement, in which the carbon atoms occupy the octahedral voids. The $Ti_3C_2T_x$ flakes are known to be terminated by a variety of functional groups, such as –OH, =O, and –F [17, 18], which enable their solubility in water.

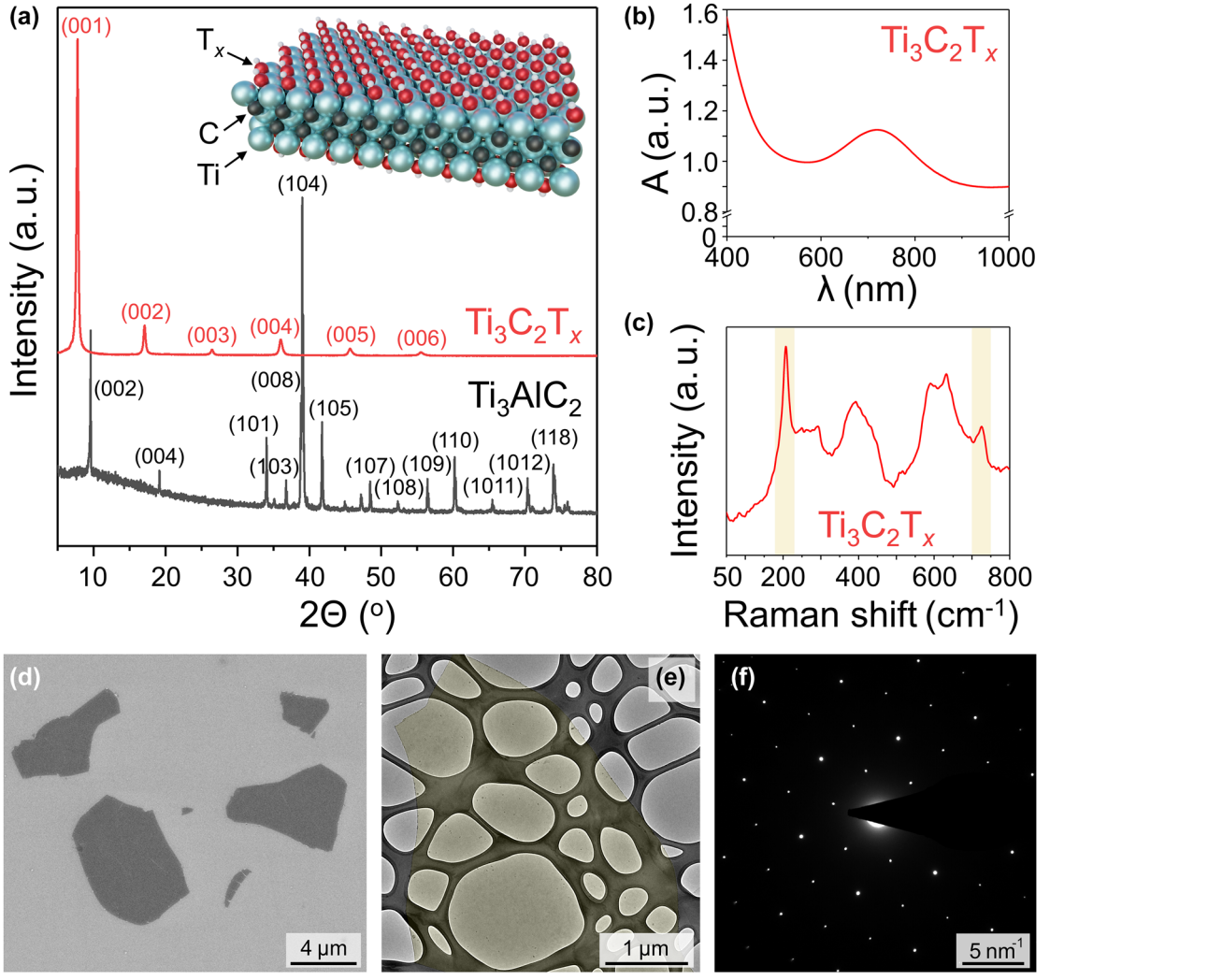

Figure 1: Characterization of $Ti_3C_2T_x$ flakes. (a) XRD patterns collected for the Ti_3AlC_2 MAX phase powder (black) and the $Ti_3C_2T_x$ MXene film (red). The inset shows the structure of a $Ti_3C_2T_x$ MXene monolayer; Ti – blue spheres, C – black spheres, the surface functional groups (T_x) are shown as –OH groups. (b) UV–vis-NIR absorption spectrum of an aqueous solution of $Ti_3C_2T_x$ MXene flakes. (c) Raman spectrum of $Ti_3C_2T_x$ MXene flakes on a gold-covered silicon substrate. (d) SEM image of $Ti_3C_2T_x$ MXene flakes on a silicon substrate. (e) TEM image of a monolayer $Ti_3C_2T_x$ flake on a lacey carbon grid. The flake is colored in yellow for clarity. (f) SAED pattern of the monolayer $Ti_3C_2T_x$ flake shown in panel (e).

The formation of $Ti_3C_2T_x$ MXene from Ti_3AlC_2 MAX phase is illustrated by the XRD patterns in Figure 1a. The black XRD pattern corresponds to Ti_3AlC_2 MAX phase and is consistent with the literature data [14]. No Ti_3AlC_2 peaks are observed in the XRD pattern of the prepared $Ti_3C_2T_x$, suggesting the absence of appreciable quantities of MAX phase residues in the synthesized MXene. The only diffraction peaks observed in the red XRD pattern are the 00l (l = 1, 2, … 6) reflections, indicating a layered structure of stacked $Ti_3C_2T_x$ MXene flakes with an interplanar distance of about 1.25 nm. This value is larger than the nominal thickness of a $Ti_3C_2T_x$ monolayer of 0.98 nm [19]. The difference in these values suggests the presence of the water molecules trapped between the layers in bulk MXene assemblies, which is consistent with the previously reported data on $Ti_3C_2T_x$ synthesized using the MILD method [14].

Figure 1b shows a UV–vis-NIR absorption spectrum of an aqueous solution of $Ti_3C_2T_x$ MXene flakes. The spectrum demonstrates that $Ti_3C_2T_x$ MXene has strong optical absorption in the visible and NIR range of spectrum. There is an absorption minimum at about 520 nm in the visible range, which is consistent with the dark green color of an aqueous solution of $Ti_3C_2T_x$ MXene [20, 21]. The absorption maximum between 700 and 800 nm was reported to represent a plasmon resonance in $Ti_3C_2T_x$ MXene [22, 23].

Figure 1c shows a Raman spectrum of $Ti_3C_2T_x$ MXene flakes deposited on a gold-covered Si/SiO_2 substrate; the measurement was performed using a 532 nm excitation laser. The spectrum shows two characteristic sharp peaks at about 208 and 726 cm^{-1}, which are highlighted in Figure 1c, that correspond to the out-of-plane A_{1g} modes of a Ti, C and T_x group vibration and a C vibration, respectively [24, 25]. The Raman spectra of MXenes were reported to strongly depend on the excitation laser energy [26]. In particular, a use of a laser with an energy coupled with the plasmon resonance peak of $Ti_3C_2T_x$ would enhance the 726 cm^{-1} peak and also reveal the resonant Raman peak around 120 cm^{-1}, which was described as an in-plane E_g group vibration of Ti, C, and T_x [24–26]. The 230 to 470 cm^{-1} range was described as a T_x region [25] containing in-plane E_g vibrations that depend on the identity of the surface functionalities. The peaks in the region from 580 to 730 cm^{-1} are primarily carbon in-plane and out-of-plane vibrations [25]. Raman spectra of $Ti_3C_2T_x$ samples strongly depend on the synthetic method and the environment of the MXene flakes [24–26]. The observed spectrum does not correspond to the Raman spectrum of Ti_3AlC_2 [27], further confirming the transformation of the precursor MAX phase to $Ti_3C_2T_x$ MXene.

The $Ti_3C_2T_x$ MXene flakes were visualized by SEM and TEM. Figure 1d shows SEM image of several $Ti_3C_2T_x$ MXene flakes that were deposited on a Si/SiO_2 substrate from an aqueous solution. The flakes look uniform and, with their lateral dimensions in a few μm range, are sufficiently large for device fabrication by EBL. Another $Ti_3C_2T_x$ MXene flake is shown in TEM image in Figure 1e. The flake was imaged on a lacey carbon TEM grid, which is seen as a dark weblike structure, and it was colored in yellow for better visibility. In the case of partial oxidation of $Ti_3C_2T_x$ flakes, microscopy analysis often reveals pinholes and elongated TiO_2 particles, which are typically observed along the flake edges [28]. In our case, the imaged flake has a uniform surface and does not display pinholes and foreign particles, suggesting the high quality of the MXene material. The high quality of the MXene flake is further confirmed by the hexagonal SAED pattern (Figure 1f), which is consistent with the structure of $Ti_3C_2T_x$ shown in the inset in Figure 1a.

The general scheme of the $Ti_3C_2T_x$ devices tested in this study is shown in Figure 2a. The scheme shows a monolayer $Ti_3C_2T_x$ flake bridging source (S) and drain (D) Cr/Au electrodes on a Si/SiO_2 substrate. The heavily p-doped Si substrate served as a global bottom gate (G) electrode in the electrical measurements. For the illumination of the devices, we used either white light of a halogen bulb or one of the lasers. We fabricated numerous devices using $Ti_3C_2T_x$ MXene flakes from three different batches and employed several different device geometries, and a negative photoresponse was observed in all experiments.

One of the tested device structures is shown in SEM image in Figure 2b, where we used interdigitated Cr/Au electrodes fabricated on a large monolayer $Ti_3C_2T_x$ MXene flake. Figure 2c shows the drain-source current (I_{DS}) –

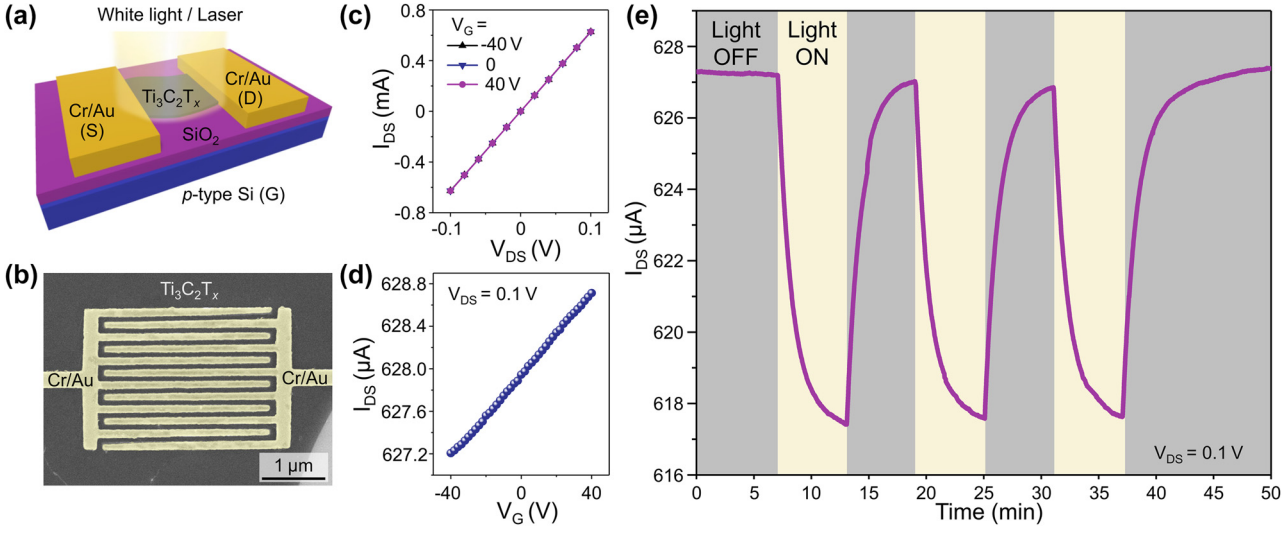

Figure 2: Negative photoresponse of monolayer $Ti_3C_2T_x$ flakes to white light. (a) Scheme of a two-terminal $Ti_3C_2T_x$ device under illumination. (b) SEM image of a device with interdigitated electrodes patterned on a monolayer $Ti_3C_2T_x$ MXene flake. The electrodes are colored in yellow for clarity. (c) $I_{DS}-V_{DS}$ curves obtained from two-terminal measurements of a $Ti_3C_2T_x$ device shown in (b) at the gate voltages of −40, 0, and 40 V. (d) $I_{DS}-V_G$ dependence for the same device measured at $V_{DS} = 0.1$ V. (e) Negative photoresponse of the same device to white light, measured at $V_{DS} = 0.1$ V and $V_G = 0$ V.

drain-source voltage (V_{DS}) dependences measured for this device at the gate voltage (V_G) of −40, 0, and 40 V. The $I_{DS}-V_{DS}$ dependences are linear, which is indicative of Ohmic contacts between the MXene flake and the Cr/Au electrodes. The $I_{DS}-V_{DS}$ dependences measured at different gate voltages nearly overlap, indicating a weak modulation of the electrical conductivity of $Ti_3C_2T_x$ by the gate voltage. Figure 2d shows transfer characteristics measured in the range of −40 V to +40 V applied to the gate electrode. The I_{DS} gradually increases when V_G sweeps from negative to positive values, indicating the n-type behavior. These $I_{DS}-V_{DS}$ and $I_{DS}-V_G$ dependences are consistent with the results of electrical measurements reported for monolayer $Ti_3C_2T_x$ MXene devices in our previous works [14, 29].

Figure 2e shows the results of photoconductivity measurements of the same monolayer $Ti_3C_2T_x$ device. We used a vacuum probe station chamber with an optical window that could be either closed or opened to enable the illumination of a device. When the window was closed and the device was kept in the dark, it showed a drain-source current of about 627 μA at V_{DS} = 0.1 V and V_G = 0 V. However, when the window was opened, enabling the illumination of the device with a white light of a halogen bulb, the drain-source current decreased by about 10 μA, demonstrating that monolayer $Ti_3C_2T_x$ MXene exhibits a negative photoresponse. This effect was completely reversible, and once the window was closed, the drain-source current increased back to the original value of about 627 μA. The optical modulation of I_{DS} in MXene devices is reproducible, which is demonstrated by three consecutive switching cycles in Figure 2e that look nearly identical.

Figure 3a shows a different device that employed a monolayer $Ti_3C_2T_x$ MXene flake from a different batch and a simpler two-terminal device geometry that is identical to the structure schematically shown in Figure 2a. This device was visualized by AFM to confirm the monolayer thickness of the MXene flake. The AFM height profile measured along the white dashed line in Figure 3a shows a step height of about 2.7 nm, see Figure 3b. It should be noted that according to theoretical calculations and high-resolution TEM studies, the nominal thickness of a $Ti_3C_2T_x$ MXene monolayer is 0.98 nm [30, 31]. However, previous AFM height measurements of monolayer $Ti_3C_2T_x$ MXene flakes on Si/SiO_2 substrates also yielded thicknesses of about 2.7 nm [14, 19, 28], and the increased height was explained by the presence of surface adsorbates, such as water molecules, that are trapped under the flakes. Similarly, increased thicknesses of monolayer flakes in

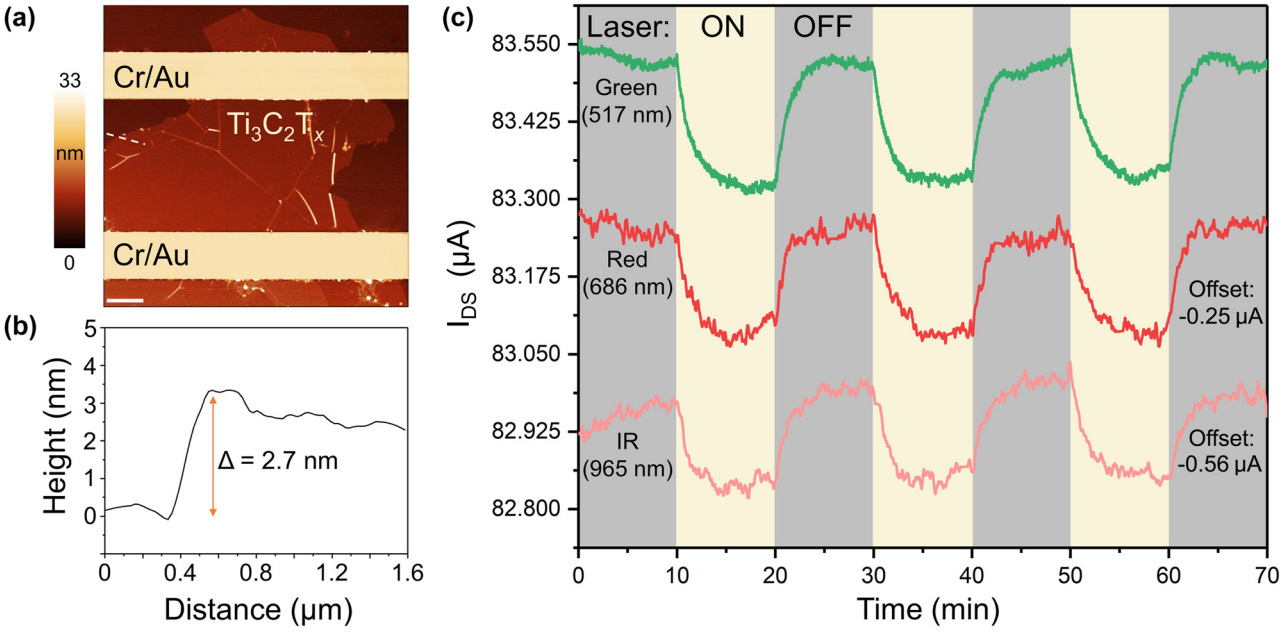

Figure 3: Negative photoresponse of monolayer $Ti_3C_2T_x$ flakes to lasers with different wavelengths. (a) False-color AFM image of a two-terminal device based on a monolayer $Ti_3C_2T_x$ MXene flake. Scale bar: 1 μm. The Cr/Au electrodes are colored in yellow for clarity. (b) AFM height profile measured along the white dashed line in panel (a). (c) The modulation of photocurrent in $Ti_3C_2T_x$ device with three different lasers, IR (965 nm), red (686 nm), and green (517 nm). All lasers were set to the same power of 3.5 mW. The measurements were performed at V_{DS} = 0.1 V and V_G = 0. The I_{DS} axis corresponds to the electrical measurement involving the green light; the other two dependences are vertically offset for clarity by −0.25 μA (red laser) and −0.56 μA (IR laser), respectively.

AFM measurements were also reported for other MXenes [32, 33] and various 2D materials [34–37].

Figure 3c shows that negative photoresponse was observed not only when the monolayer $Ti_3C_2T_x$ MXene devices were illuminated with white light, but also in experiments involving different lasers with wavelengths in the visible and near-infrared range of spectrum. We used lasers with wavelengths of 517, 686 and 965 nm, at all of which $Ti_3C_2T_x$ MXene exhibits a considerable optical absorption. Figure 3c shows that the drain-source current reproducibly decreased when the device was illuminated with any of the three lasers and then restored back to the original value once the optical window was closed. The negative photoresponse observed in these experiments can be explained by the metallic nature of the electrical conductivity of $Ti_3C_2T_x$ MXene [38, 39], which decreases under the illumination due to increased scattering. While we did not have access to a laser with a wavelength in the 700–800 nm range that would match the plasmon resonance in $Ti_3C_2T_x$ MXene [22, 23], it would be interesting to investigate whether the use of such laser would result in an enhanced negative photoresponse due to an increased absorption.

The negative photoresponse makes metallic $Ti_3C_2T_x$ MXene very different from a great variety of semiconducting 2D materials that had been extensively studied for photodetector applications in recent years and exhibited positive photoresponse [40–46]. The negative photoresponse in pristine $Ti_3C_2T_x$ is also very different from the positive photoresponse of the partially oxidized material, in which the oxidation of $Ti_3C_2T_x$ results in the formation of TiO_2, a wide bandgap semiconductor that could be excited with UV light [8]. Collectively, these results suggest that $Ti_3C_2T_x$ could exhibit a tunable photoresponse that would depend on the degree of oxidation of MXene.

4 Conclusions

In summary, we demonstrated that individual monolayer $Ti_3C_2T_x$ MXene flakes exhibit a negative photoresponse in the visible and near-infrared spectrum range. This information is important for several areas of MXene research. First, there are ongoing studies of MXenes that aim to determine their intrinsic electrical properties, such as electrical conductivity [14, 21, 29, 32] and breakdown current density [29, 33]. The knowledge of these properties is necessary for advancing a variety of MXene applications ranging from energy storage [47] and transparent conductive electrodes [48, 49] to interconnects [29, 33] and gas sensors [28, 39]. Since this study establishes that the conductivity of $Ti_3C_2T_x$ (and likely, other MXenes) is affected by light, it should be important for the future electrical property characterizations of MXenes to indicate whether the measurements were performed under illumination or in the dark for a more accurate comparison of results from different studies. Second, the negative photoresponse of $Ti_3C_2T_x$ MXene could be responsible for a similar effect reported for MXene heterostructures with other materials [9, 10]. Finally, the negative photoresponse of $Ti_3C_2T_x$ should be taken into account in MXene applications that directly employ light–matter interactions, such as photodetectors and solar cells [2–4, 11].

Author contributions: N. S. V., S. B. and A. T. contributed equally to this work. S. B. synthesized $Ti_3C_2T_x$ MXene and performed the materials characterization. N. S. V. and A. T. fabricated $Ti_3C_2T_x$ MXene devices and performed the electrical measurements. N. S. V. and A. S. wrote the manuscript. A. S. concieved the idea of this study and supervised the project.

Research funding: The work was supported by the Nebraska Center for Energy Sciences Research (NCESR). Some experiments were performed using the instrumentation at the Nebraska Nanoscale Facility, which is supported by the National Science Foundation (ECCS-2025298) and the Nebraska Research Initiative.

Conflict of interest statement: The authors declare no conflicts of interest regarding this article.

References

[1] B. Anasori and Y. Gogotsi, Eds. *2D Metal Carbides and Nitrides (MXenes): Structure, Properties and Applications*, Cham, Springer International Publishing, 2019.

[2] H. Xu, A. Ren, J. Wu, and Z. Wang, "Recent advances in 2D MXenes for photodetection," *Adv. Funct. Mater.*, vol. 30, p. 2000907, 2020.

[3] Z. Liu and H. N. Alshareef, "MXenes for optoelectronic devices," *Adv. Electron. Mater.*, vol. 7, p. 2100295, 2021.

[4] X. Zhang, J. Shao, C. Yan, et al., "A review on optoelectronic device applications of 2D transition metal carbides and nitrides," *Mater. Des.*, vol. 200, p. 109452, 2021.

[5] D. Zhang, D. Shah, A. Boltasseva, and Y. Gogotsi, "MXenes for photonics," *ACS Photonics*, vol. 9, pp. 1108–1116, 2022.

[6] L. Gao, C. Ma, S. Wei, A. V. Kuklin, H. Zhang, and H. Ågren, "Applications of few-layer Nb_2C MXene: narrow-band photodetectors and femtosecond mode-locked fiber lasers," *ACS Nano*, vol. 15, pp. 954–965, 2021.

[7] D. B. Velusamy, J. K. El-Demellawi, A. M. El-Zohry, et al., "MXenes for plasmonic photodetection," *Adv. Mater.*, vol. 31, p. 1807658, 2019.

[8] S. Chertopalov and V. N. Mochalin, "Environment-sensitive photoresponse of spontaneously partially oxidized Ti_3C_2 MXene thin films," *ACS Nano*, vol. 12, pp. 6109–6116, 2018.
[9] T. Jiang, Y. Huang, and X. Meng, "CdS core-Au/MXene-based photodetectors: positive deep-UV photoresponse and negative UV–Vis-NIR photoresponse," *Appl. Surf. Sci.*, vol. 513, p. 145813, 2020.
[10] J. Zhu, H. Wang, L. Ma, and G. Zou, "Observation of ambipolar photoresponse from 2D MoS_2/MXene heterostructure," *Nano Res.*, vol. 14, pp. 3416–3422, 2021.
[11] A. Agresti, A. Pazniak, S. Pescetelli, et al., "Titanium-carbide MXenes for work function and interface engineering in perovskite solar cells," *Nat. Mater.*, vol. 18, pp. 1228–1234, 2019.
[12] C. Hou and H. Yu, "ZnO/$Ti_3C_2T_x$ monolayer electron transport layers with enhanced conductivity for highly efficient inverted polymer solar cells," *Chem. Eng. J.*, vol. 407, p. 127192, 2021.
[13] Y. Gogotsi and B. Anasori, "The rise of MXenes," *ACS Nano*, vol. 13, pp. 8491–8494, 2019.
[14] A. Lipatov, M. Alhabeb, M. R. Lukatskaya, A. Boson, Y. Gogotsi, and A. Sinitskii, "Effect of synthesis on quality, electronic properties and environmental stability of individual monolayer Ti_3C_2 MXene flakes," *Adv. Electron. Mater.*, vol. 2, p. 1600255, 2016.
[15] A. Sinitskii, A. Dimiev, D. V. Kosynkin, and J. M. Tour, "Graphene nanoribbon devices produced by oxidative unzipping of carbon nanotubes," *ACS Nano*, vol. 4, pp. 5405–5413, 2010.
[16] A. Lipatov, N. S. Vorobeva, T. Li, A. Gruverman, and A. Sinitskii, "Using light for better programming of ferroelectric devices: optoelectronic MoS_2-Pb(Zr, Ti)O_3 memories with improved on–off ratios," *Adv. Electron. Mater.*, vol. 7, p. 2001223, 2021.
[17] J. Halim, K. M. Cook, M. Naguib, et al., "X-ray photoelectron spectroscopy of select multi-layered transition metal carbides (MXenes)," *Appl. Surf. Sci.*, vol. 362, pp. 406–417, 2016.
[18] M. Seredych, C. E. Shuck, D. Pinto, et al., "High-temperature behavior and surface chemistry of carbide MXenes studied by thermal analysis," *Chem. Mater.*, vol. 31, pp. 3324–3332, 2019.
[19] A. Lipatov, H. Lu, M. Alhabeb, et al., "Elastic properties of 2D $Ti_3C_2T_x$ MXene monolayers and bilayers," *Sci. Adv.*, vol. 4, p. eaat0491, 2018.
[20] M. Alhabeb, K. Maleski, B. Anasori, et al., "Guidelines for synthesis and processing of two-dimensional titanium carbide ($Ti_3C_2T_x$ MXene)," *Chem. Mater.*, vol. 29, pp. 7633–7644, 2017.
[21] K. Hantanasirisakul, M. Alhabeb, A. Lipatov, et al., "Effects of synthesis and processing on optoelectronic properties of titanium carbonitride MXene," *Chem. Mater.*, vol. 31, pp. 2941–2951, 2019.
[22] D. B. Lioi, P. R. Stevenson, B. T. Seymour, et al., "Simultaneous ultrafast transmission and reflection of nanometer-thick $Ti_3C_2T_x$ MXene films in the visible and near-infrared: implications for energy storage, electromagnetic shielding, and laser systems," *ACS Appl. Nano Mater.*, vol. 3, pp. 9604–9609, 2020.
[23] K. Maleski, C. E. Shuck, A. T. Fafarman, and Y. Gogotsi, "The broad chromatic range of two-dimensional transition metal carbides," *Adv. Opt. Mater.*, vol. 9, p. 2001563, 2021.
[24] A. Sarycheva, M. Shanmugasundaram, A. Krayev, and Y. Gogotsi, "Tip-enhanced Raman scattering imaging of single- to few-layer $Ti_3C_2T_x$ MXene," *ACS Nano*, vol. 16, pp. 6858–6865, 2022.
[25] A. Sarycheva and Y. Gogotsi, "Raman spectroscopy analysis of the structure and surface chemistry of $Ti_3C_2T_x$ MXene," *Chem. Mater.*, vol. 32, pp. 3480–3488, 2020.
[26] D. B. Lioi, G. Neher, J. E. Heckler, et al., "Electron-withdrawing effect of native terminal groups on the lattice structure of $Ti_3C_2T_x$ MXenes studied by resonance Raman scattering: implications for embedding MXenes in electronic composites," *ACS Appl. Nano Mater.*, vol. 2, pp. 6087–6091, 2019.
[27] V. Presser, M. Naguib, L. Chaput, A. Togo, G. Hug, and M. W. Barsoum, "First-order Raman scattering of the MAX phases: Ti_2AlN, $Ti_2AlC_{0.5}N_{0.5}$, Ti_2AlC, $(Ti_{0.5}V_{0.5})_2AlC$, V_2AlC, Ti_3AlC_2, and Ti_3GeC_2," *J. Raman Spectrosc.*, vol. 43, pp. 168–172, 2012.
[28] H. Pazniak, I. A. Plugin, M. J. Loes, et al., "Partially oxidized $Ti_3C_2T_x$ MXenes for fast and selective detection of organic vapors at part-per-million concentrations," *ACS Appl. Nano Mater.*, vol. 3, pp. 3195–3204, 2020.
[29] A. Lipatov, A. Goad, M. J. Loes, et al., "High electrical conductivity and breakdown current density of individual monolayer $Ti_3C_2T_x$ MXene flakes," *Matter*, vol. 4, pp. 1413–1427, 2021.
[30] M. Ghidiu, M. R. Lukatskaya, M. Q. Zhao, Y. Gogotsi, and M. W. Barsoum, "Conductive two-dimensional titanium carbide 'clay' with high volumetric capacitance," *Nature*, vol. 516, pp. 78–81, 2014.
[31] X. Wang, X. Shen, Y. Gao, Z. Wang, R. Yu, and L. Chen, "Atomic-scale recognition of surface structure and intercalation mechanism of Ti_3C_2X," *J. Am. Chem. Soc.*, vol. 137, pp. 2715–2721, 2015.
[32] A. Lipatov, M. Alhabeb, H. Lu, et al., "Electrical and elastic properties of individual single-layer $Nb_4C_3T_x$ MXene flakes," *Adv. Electron. Mater.*, vol. 6, p. 1901382, 2020.
[33] A. Lipatov, M. J. Loes, N. S. Vorobeva, et al., "High breakdown current density in monolayer $Nb_4C_3T_x$ MXene," *ACS Mater. Lett.*, vol. 3, pp. 1088–1094, 2021.
[34] K. S. Novoselov, D. Jiang, F. Schedin, et al., "Two-dimensional atomic crystals," *Proc. Natl. Acad. Sci. U. S. A.*, vol. 102, pp. 10451–10453, 2005.
[35] K. Xu, P. Cao, and J. R. Heath, "Graphene visualizes the first water adlayers on mica at ambient conditions," *Science*, vol. 329, pp. 1188–1191, 2010.
[36] O. Ochedowski, B. K. Bussmann, and M. Schleberger, "Graphene on mica – intercalated water trapped for life," *Sci. Rep.*, vol. 4, p. 6003, 2014.
[37] H. Coy Diaz, R. Addou, and M. Batzill, "Interface properties of CVD grown graphene transferred onto MoS_2(0001)," *Nanoscale*, vol. 6, pp. 1071–1078, 2014.
[38] J. L. Hart, K. Hantanasirisakul, A. C. Lang, et al., "Control of MXenes' electronic properties through termination and intercalation," *Nat. Commun.*, vol. 10, p. 522, 2019.

[39] S. J. Kim, H. J. Koh, C. E. Ren, et al., "Metallic $Ti_3C_2T_x$ MXene gas sensors with ultrahigh signal-to-noise ratio," *ACS Nano*, vol. 12, pp. 986–993, 2018.
[40] C. Xie, C. Mak, X. Tao, and F. Yan, "Photodetectors based on two-dimensional layered materials beyond graphene," *Adv. Funct. Mater.*, vol. 27, p. 1603886, 2017.
[41] H. Qiao, Z. Huang, X. Ren, et al., "Self-Powered photodetectors based on 2D materials," *Adv. Opt. Mater.*, vol. 8, p. 1900765, 2020.
[42] T. Fan, Z. Xie, W. Huang, Z. Li, and H. Zhang, "Two-dimensional non-layered selenium nanoflakes: facile fabrications and applications for self-powered photo-detector," *Nanotechnology*, vol. 30, p. 114002, 2019.
[43] S. J. Gilbert, H. Yi, J. S. Chen, et al., "Effect of band symmetry on photocurrent production in quasi-one-dimensional transition-metal trichalcogenides," *ACS Appl. Mater. Interfaces*, vol. 12, pp. 40525–40531, 2020.
[44] Y. Zhang, P. Huang, J. Guo, et al., "Graphdiyne-based flexible photodetectors with high responsivity and detectivity," *Adv. Mater.*, vol. 32, p. 2001082, 2020.
[45] N. S. Vorobeva, A. Lipatov, A. Torres, et al., "Anisotropic properties of quasi-1D In_4Se_3: mechanical exfoliation, electronic transport, and polarization-dependent photoresponse," *Adv. Funct. Mater.*, vol. 31, p. 2106459, 2021.
[46] Z. Guo, R. Cao, H. Wang, et al., "High-performance polarization-sensitive photodetectors on two-dimensional β-InSe," *Natl. Sci. Rev.*, vol. 9, p. nwab098, 2022.
[47] B. Anasori, M. R. Lukatskaya, and Y. Gogotsi, "2D metal carbides and nitrides (MXenes) for energy storage," *Nat. Rev. Mater.*, vol. 2, p. 16098, 2017.
[48] J. Halim, M. R. Lukatskaya, K. M. Cook, et al., "Transparent conductive two-dimensional titanium carbide epitaxial thin films," *Chem. Mater.*, vol. 26, pp. 2374–2381, 2014.
[49] K. Hantanasirisakul, M. Q. Zhao, P. Urbankowski, et al., "Fabrication of $Ti_3C_2T_x$ MXene transparent thin films with tunable optoelectronic properties," *Adv. Electron. Mater.*, vol. 2, p. 1600050, 2016.